EUROPEAN COOPERATION
IN THE FIELD OF SCIENTIFIC
AND TECHNICAL RESEARCH

EURO-COST

IC1004 TD(15)12067
Dublin, Ireland
Jan. 28-30, 2015

SOURCE: Signal Processing and Speech Communication
Laboratory, Graz University of Technology, Austria

Robust and Accurate Indoor Localization using Channel Information

Paul Meissner, Erik Leitinger, and Klaus Witrisal
Inffeldgasse 16c
A-8010 Graz
Austria
Phone: +43 316 873 4363
Fax: +43 316 873 104363
Email: paul.meissner@tugraz.at, witrisal@tugraz.at

Robust and Accurate Indoor Localization using Channel Information

Paul Meissner, Erik Leitinger, and Klaus Witrisal

***Abstract*—In a radio propagation channel, deterministic reflections carry important position-related information. With the help of prior knowledge such as a floor plan, this information can be exploited for indoor localization. This paper shows that information about the channel parameters is the crucial ingredient to make the localization robust and accurate. The variances of the ranges corresponding to deterministic, specular multipath components can be estimated either from a few training signals at known positions or online during tracking using estimated positions. These range variances are useful in two ways: First, the Cramer-Rao Lower Bound (CRLB) of the position error can be computed using measurement signals, which allows to characterize an environment in terms of localization accuracy. Second, the range variances can be fed to a tracking filter as observation noise model. We present tracking results for ultra-wideband measurements in a partial non-line-of-sight environment. At a bandwidth of $2\,$GHz, an accuracy of $4\,$cm can be achieved for over $90\,\%$ of the positions if additional channel information is available. Otherwise, this accuracy is only possible for about $45\,\%$ of the positions. The covariance of the estimation matches closely to the corresponding Cramér-Rao Lower Bound.**

I. Introduction

Robustness and accuracy are key requirements of indoor localization systems. We define robustness as the percentage of cases in which a system can achieve its given potential accuracy. Due to their fine time resolution, range-based ultra-wideband (UWB) systems provide accurate distance estimates between anchors and the agent to be localized [3]. However, a non-line-of-sight (NLOS) situation can decrease the robustness due to biased range estimates. We have proposed an approach called multipath-assisted indoor navigation and tracking (MINT) to enhance the robustness [4], [5]. It makes use of the floor plan to associate multipath components (MPCs) to the surrounding geometry.

In this paper, we show how position-related information can be used efficiently as additional prior information. Channel parameters describing the reliability of the reflected MPCs [5], [6] are estimated from a few training signals with an agent at known positions and used in the tracking filter as measurement noise model. For a navigating agent, awareness to the uncertainty of the available information is crucial for the tracking performance both in theoretic [7] and in practical settings [8]. Taking into account diffuse multipath (DM) allows for much more realistic performance indications [9], especially in dense multipath environments.

[10]

The main contributions of this letter are:

- We show that a multipath-assisted tracking approach can be made aware of the relevance of specific deterministic MPCs in an environment.
- Using measurements, we show that centimeter-level accuracy can be achieved robustly also in NLOS conditions.
- The estimated uncertainties of the deterministic MPCs can be used to obtain a realistic prediction of the localization performance using the CRLB.

Notation: The symbols $*$, $(\cdot)^T$, $(\cdot)^*$, $\mathbb{E}\{\cdot\}$, $\Re\{\cdot\}$, and $\mathbf{I}_N$ denote convolution, transposition, conjugation, expectation, real part, and an identity matrix of dimension N, respectively.

II. Tracking and Channel Estimation

A. Signal and Geometry Models

We aim at tracking a mobile agent in an environment with J anchors at known positions. The signal between the j-th anchor and the agent at the position $\mathbf{p}_\ell$ is modeled as [5]

$$r_\ell^{(j)}(t) = \sum_{k=1}^{K_\ell^{(j)}} \alpha_{k,\ell}^{(j)} s(t-\tau_{k,\ell}^{(j)}) + s(t) * \nu_\ell^{(j)}(t) + w(t). \quad (1)$$

The sets $\{\alpha_{k,\ell}^{(j)}\}$ and $\{\tau_{k,\ell}^{(j)}\}$ are the complex amplitudes and delays of the k-th deterministic MPC, respectively. The signal $s(t)$ denotes the transmitted pulse shape with effective pulse duration T_p. The random process $\nu_\ell^{(j)}(t)$ denotes DM and is modeled as a Gaussian process with auto-covariance $\mathbb{E}\{\nu_\ell^{(j)}(\tau)[\nu_\ell^{(j)}(u)]^*\} = S_{\nu,\ell}^{(j)}(\tau)\delta(\tau-u)$, where $S_{\nu,\ell}^{(j)}(\tau)$ is the power delay profile (PDP) of the DM. The signal $w(t)$ denotes white Gaussian measurement noise with double-sided power spectral density (PSD) of $N_0/2$.

The delays of the $K_\ell^{(j)}$ deterministic MPCs are modeled geometrically using mirror images of the j-th anchor with respect to the corresponding walls, introducing so-called virtual anchors (VAs) [4], [11]. Fig. 1 shows two examples of such VAs. It can be seen that the distance from the agent's position $\mathbf{p}_\ell$ to the k-th VA at $\mathbf{p}_k^{(j)}$ corresponds to the delay $\tau_{k,\ell}^{(j)} = \frac{1}{c} d_{k,\ell}^{(j)} = \frac{1}{c}\|\mathbf{p}_\ell - \mathbf{p}_k^{(j)}\|$ of the corresponding MPC, where c denotes the speed of light. For the whole scenario, a set $\mathcal{A}^{(j)}$ of all potential VAs of the j-th anchor can be constructed. Higher-order VAs are obtained by mirroring again lower-order VAs with respect to reflectors. Using

P. Meissner, E. Leitinger and K. Witrisal are with Graz University of Technology, Graz, Austria, email: paul.meissner@tugraz.at.

The authors thank Manuel Lafer for his help in performing the measurement campaign. This TD is an extended version of [1]. Further information on the topic can be found in the TD [2].

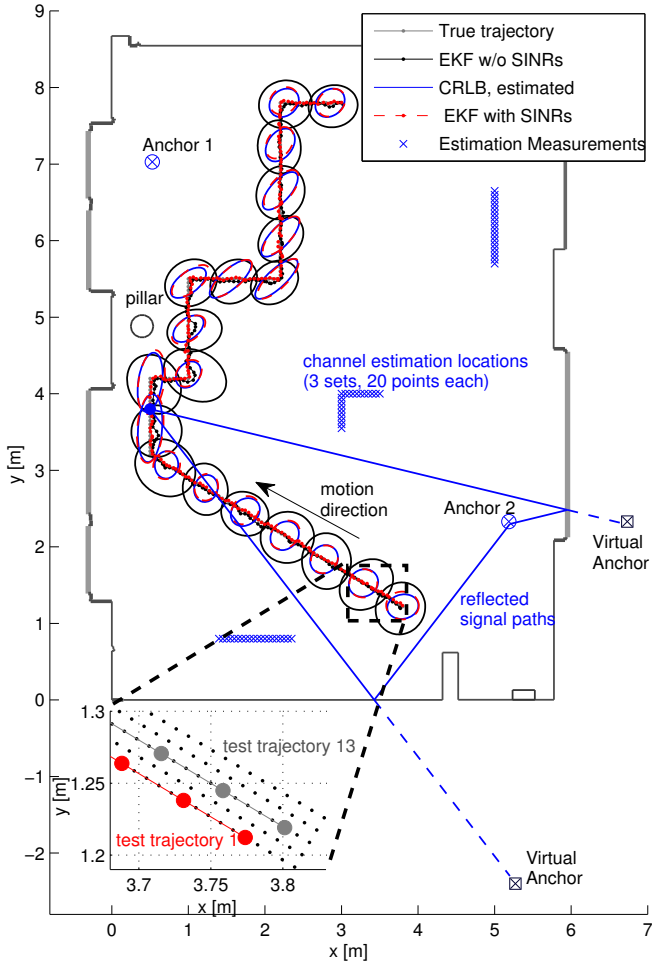

Fig. 1. Floor plan of the evaluation scenario, bold gray lines denote windows and other lines illustrate walls made of different materials. Examples for true and estimated agent trajectories are shown, the former is hidden beneath the others. The bottom contains a close-up of the trajectories, illustrating the 1-cm-spaced grid, out of which 25 5-cm-spaced trajectories are obtained. Two physical anchors are indicated with examples for virtual anchors modeling reflections from walls. Ellipses denote 20-fold standard deviations of the trackers as well as the respective 20-fold CRLB, as described in the text.

optical ray-tracing, the set of visible VAs can be computed for position $\mathbf{p}_\ell$ as

$$\mathcal{A}_\ell^{(j)} = \{\mathbf{p}_{\ell,1}^{(j)}, \ldots, \mathbf{p}_{\ell,K_\ell^{(j)}}^{(j)}\} = \{\mathbf{p}_k^{(j)} : f_{\mathrm{vis}}(\mathbf{p}_k^{(j)}, \mathbf{p}_\ell) = 1\} \tag{2}$$

where the ray-tracing is expressed by the function

$$f_{\mathrm{vis}}(\mathbf{p}_k^{(j)}, \mathbf{p}) = \begin{cases} 1, & \text{if VA } \mathbf{p}_k^{(j)} \text{ is visible at } \mathbf{p} \\ 0, & \text{else.} \end{cases} \tag{3}$$

B. Tracking Algorithm

In a first step, the location-dependent parameters, i.e. the arrival times of the deterministic MPCs, are estimated from the received signal modeled by (1). The arrival time estimation at position ℓ is realized as an iterative least-squares approximation of the received signal

$$\hat{\tau}_{k,\ell}^{(j)} = \arg\min_\tau \int_0^T \left| r_\ell^{(j)}(t) - \hat{r}_{\ell,k-1}^{(j)}(t) - \hat{\alpha}(\tau) s(t-\tau) \right|^2 dt \tag{4}$$

using a template signal $\hat{r}_{\ell,k}^{(j)}(t) = \sum_{k'=1}^{k} \hat{\alpha}_{k',\ell}^{(j)} s(t - \hat{\tau}_{k',\ell}^{(j)})$ for all MPCs up to the k-th. The path amplitudes are nuisance parameters, estimated using a projection of $r_\ell^{(j)}(t)$ onto a unit energy pulse $s(t)$ as

$$\hat{\alpha}(\tau) = \int_0^T [r_\ell^{(j)}(t)]^* s(t-\tau) dt; \quad \hat{\alpha}_{k,\ell}^{(j)} = \hat{\alpha}(\hat{\tau}_{k,\ell}^{(j)}). \tag{5}$$

The number of estimated MPCs $\hat{K}_\ell^{(j)}$ should be chosen according to the number of expected specular paths in an environment. With the assumptions of separable MPCs and white noise, (4) and (5) correspond to a maximum-likelihood (ML) estimation of the deterministic MPCs.

The tracking is done as in [4] using an EKF with data association (DA), which is necessary since the estimated MPC arrival times in (4) are not associated to the VAs. We choose a simple linear Gaussian constant-velocity motion model

$$\begin{aligned} \mathbf{x}_{\ell+1} =& \mathbf{F}\mathbf{x}_\ell + \mathbf{G}\mathbf{n}_{\mathrm{a},\ell} \\ =& \begin{bmatrix} 1 & 0 & \Delta T & 0 \\ 0 & 1 & 0 & \Delta T \\ 0 & 0 & 1 & 0 \\ 0 & 0 & 0 & 1 \end{bmatrix} \mathbf{x}_\ell + \begin{bmatrix} \frac{\Delta T^2}{2} & 0 \\ 0 & \frac{\Delta T^2}{2} \\ \Delta T & 0 \\ 0 & \Delta T \end{bmatrix} \mathbf{n}_{\mathrm{a},\ell}. \end{aligned} \tag{6}$$

The state vector $\mathbf{x}_\ell$ of the agent contains position $\mathbf{p}_\ell$ and the velocity vector, and ΔT is the update rate. The driving acceleration noise term $\mathbf{n}_{\mathrm{a},\ell}$ with zero mean and covariance matrix $\mathbf{Q} = \sigma_a^2 \mathbf{G}\mathbf{G}^T$ models motion changes that deviate from the constant-velocity assumption.

For the measurement update of the EKF, the set of expected VAs is calculated for the DA at the predicted position $\mathbf{p}_\ell^-$ using (2) for each anchor, yielding sets $\bar{\mathcal{A}}_\ell^{(j)}$. At this time, prior information such as a set $\tilde{\mathcal{A}}^{(j)}$ defining *relevant* VAs can be used to restrict the set of expected VAs, resulting in $\bar{\mathcal{A}}_\ell^{(j)} \cap \tilde{\mathcal{A}}^{(j)}$. The corresponding expected path delays are then matched to the estimated arrival times (4) such that the cumulative distance of estimated and expected delays is minimized, yielding sets of associated VAs $\mathcal{A}_{\ell,\mathrm{ass}}^{(j)}$. The association is done using a constrained optimal subpattern assignment approach [4], [12], where the constraint is that associations at a distance larger than a given maximum ranging uncertainty, the so-called cut-off distance d_c, are discarded.

After joining information from all anchors, $\mathcal{A}_{\ell,\mathrm{ass}} = \bigcup_j \mathcal{A}_{\ell,\mathrm{ass}}^{(j)}$, the corresponding distance estimates are stacked in the EKF's measurement input vector which is *modeled* as

$$\mathbf{z}_\ell = \left[\ldots, \|\mathbf{p}_k^{(j)} - \mathbf{p}_\ell\|, \ldots\right]^T + \mathbf{n}_{z,\ell}, \ \mathbf{p}_k^{(j)} \in \mathcal{A}_{\ell,\mathrm{ass}}. \tag{7}$$

The measurement noise $\mathbf{n}_{z,\ell}$ is assumed to be zero-mean multivariate Gaussian. The choice of the measurement noise covariance matrix $\mathbf{R}_\ell$ depends on the amount of prior

information. If a-priori estimates of the range estimation uncertainties $\mathrm{var}\left\{\hat{d}_{k,\ell}^{(j)}\right\}$ are available for a set of VAs, then

$$\mathbf{R}_\ell = \mathrm{diag}\left\{\mathrm{var}\left\{\hat{d}_{k,\ell}^{(j)}\right\}\right\} \quad \forall\, k,j : \mathbf{p}_k^{(j)} \in \mathcal{A}_{\ell,\mathrm{ass}}. \tag{8}$$

Otherwise, an overall uncertainty σ_d^2 is used, i.e.

$$\mathbf{R}_\ell = \sigma_\mathrm{d}^2 \mathbf{I}_{|\mathcal{A}_{\ell,\mathrm{ass}}|}. \tag{9}$$

Fig. 2 shows an overview over the tracking scheme.

C. Position-Related Information and its Estimation

In [5], we have derived the Cramèr Rao Lower Bound (CRLB) for positioning based on the signal model (1) and the VAs. With the assumption of no path overlap, i.e. the MPCs are orthogonal, the equivalent Fisher information matrix (EFIM) for position $\mathbf{p}_\ell$ [13] is given as

$$\mathbf{J}_{\mathbf{p}_\ell} = \sum_{j=1}^{J}\sum_{k=1}^{K_\ell^{(j)}} \mathrm{J}_r(d_{k,\ell}^{(j)})\mathbf{J}_r(\phi_{k,\ell}^{(j)}). \tag{10}$$

where the ranging direction matrix $\mathbf{J}_r(\phi_{k,\ell}^{(j)})$ determines the direction $\phi_{k,\ell}^{(j)}$ of the information of the k-th MPC, since it is spanned by the outer product of the unit vector pointing from the k-th VA at $\mathbf{p}_k^{(j)}$ to the agent at $\mathbf{p}_\ell$ with itself [5]. It is scaled by the Fisher information contained in the signal $r_\ell^{(j)}(t)$ about the path length $d_{k,\ell}^{(j)}$. Its inverse is the CRLB for the variance of an unbiased range estimate $\hat{d}_{k,\ell}^{(j)}$

$$\mathrm{J}_r^{-1}(d_{k,\ell}^{(j)}) = \left(\frac{8\pi^2\beta^2}{c^2}\mathrm{SINR}_{k,\ell}^{(j)}\right)^{-1} \leq \mathrm{var}\left\{\hat{d}_{k,\ell}^{(j)}\right\}. \tag{11}$$

Here, β denotes the effective (root mean square) bandwidth of $s(t)$ and the signal-to-interference-and-noise-ratio (SINR) of the k-th MPC at $\mathbf{p}_\ell$ is defined as

$$\mathrm{SINR}_{k,\ell}^{(j)} = \frac{|\alpha_{k,\ell}^{(j)}|^2}{N_0 + T_\mathrm{p} S_{\nu,\ell}^{(j)}(\tau_{k,\ell}^{(j)})}. \tag{12}$$

1) Estimation using Training Measurements at known Positions: In [6], we have derived an estimator for the average $\mathrm{SINR}_k^{(j)}$, averaged over positions within a confined spatial region in which propagation characteristics such as the PDP of the DM are assumed to be stationary. However, there is only a limited number of MPCs visible within such a region. To increase this number, we use measurements at N_seg sets of points $\{\mathbf{p}_\ell : \ell \in \mathcal{P}_i\}$, where $\mathcal{P}_i,\ i = 1,\ldots,N_\mathrm{seg}$, collects the indices of the points. Within each set, propagation characteristics are again assumed to be stationary and an $\widehat{\mathrm{SINR}}_k^{(j,i)}$ can be estimated. For this, we have to take into account the *observability* of the corresponding VA. We define the subsets

$$\begin{aligned}\mathcal{P}_k^{(j,i)} =& \{\ell \in \mathcal{P}_i : f_\mathrm{vis}(\mathbf{p}_\ell, \mathbf{p}_k^{(j)}) = 1 \wedge \\ & |\tau_{k,\ell}^{(j)} - \tau_{k',\ell}^{(j)}| > T_\mathrm{p}\ \forall\ k' \neq k,\ \mathbf{p}_{k'}^{(j)} \in \mathcal{A}_\ell^{(j)}\}\end{aligned} \tag{13}$$

with cardinality $N_k^{(j,i)}$. The conditions in (13) imply that the k-th VA is visible at $\mathbf{p}_\ell$ and there is no path overlap [5], [13] with any other VA-modeled MPC.

The overall aim is to take into account the uncertainty of the MPCs in an environment, both w.r.t. the path length estimation and also w.r.t. the position of the VAs, as these are subject to floor plan uncertainties. For the estimation of a *global* range uncertainty of a specific MPC, which is necessary to be useful as a location-independent noise model (8), we propose the weighted mean of the local uncertainties

$$\widehat{\mathrm{var}}\left\{\hat{d}_k^{(j)}\right\} = \frac{1}{\sum_{i=1}^{N_\mathrm{seg}} N_k^{(j,i)}} \sum_{i=1}^{N_\mathrm{seg}} N_k^{(j,i)} \widehat{\mathrm{var}}\left\{\hat{d}_{k,\ell}^{(j)} : \ell \in \mathcal{P}_k^{(j,i)}\right\}. \tag{14}$$

The $\widehat{\mathrm{var}}\left\{\hat{d}_{k,\ell}^{(j)}\right\}$ is obtained from an SINR estimate and (11). This and the use of (14) are motivated by assuming the range estimates $\hat{d}_{k,\ell}^{(j)}$ to be Gaussian distributed, which is justified by the fact that (4) is an approximation for the according ML estimator and as such is asymptotically efficient, i.e. $\hat{d}_{k,\ell}^{(j)} \sim \mathcal{N}\left(d_{k,\ell}^{(j)}; \mathrm{J}_r^{-1}(d_{k,\ell}^{(j)})\right)$.

The VA positions are corrected using a prior $p(\tilde{\mathbf{p}}_k^{(j)})$ for the k-th VA. This leads to the MAP estimate

$$\hat{\mathbf{p}}_k^{(j)} = \arg\max_{\tilde{\mathbf{p}}_k^{(j)}} \ln p(\mathbf{r}^{(j)}(t)|\tilde{\mathbf{p}}_k^{(j)}) + \ln p(\tilde{\mathbf{p}}_k^{(j)}) \tag{15}$$

with a likelihood function that evaluates the contribution of the k-th VA to all estimation signals $\mathbf{r}^{(j)}(t)$ (c.f. [5] but neglecting the whitening to account for the DM)

$$\begin{aligned}\ln p(\mathbf{r}^{(j)}(t)|\tilde{\mathbf{p}}_k^{(j)}) \propto & \frac{2}{N_0}\sum_{i=1}^{N_\mathrm{seg}}\sum_{\ell\in\mathcal{P}_k^{(j,i)}}\int_0^T \Re\left\{[r_\ell^{(j)}(t)]^* \tilde{s}_{k,\ell}^{(j)}(t)\right\} dt \\ & - \frac{1}{N_0}\int_0^T |\tilde{s}_{k,\ell}^{(j)}(t)|^2 dt.\end{aligned} \tag{16}$$

Here, $\tilde{s}_{k,\ell}^{(j)}(t) = \tilde{\alpha}_{k,\ell}^{(j)} s(t - \tilde{\tau}_{k,\ell}^{(j)})$ is a template signal where $\tilde{\tau}_{k,\ell}^{(j)} = \frac{1}{c}\|\tilde{\mathbf{p}}_k^{(j)} - \mathbf{p}_\ell\|$ and the MPC amplitudes are again nuisance parameters and estimated using (5). The vector of received signals for the estimation is given as

$$\mathbf{r}^{(j)}(t) = [r_{\ell\in\mathcal{P}_1}^{(j)}(t),\ \ldots,\ r_{\ell\in\mathcal{P}_{N_\mathrm{seg}}}^{(j)}(t)]^T. \tag{17}$$

With the signal model in (1) and $\hat{m}_{1,k}^{(j,i)}$ and $\hat{m}_{2,k}^{(j,i)}$ denoting estimates of the first and second central moments of the energy samples $|\tilde{\alpha}_{k,\ell}^{(j)}|^2$ for $\ell \in \mathcal{P}_k^{(j,i)}$, the corresponding average SINRs are estimated as [6]

$$\widehat{\mathrm{SINR}}_k^{(j,i)} = \left(\frac{\hat{m}_{1,k}^{(j,i)}}{\sqrt{\hat{m}_{1,k}^{(j,i)^2} - \hat{m}_{2,k}^{(j,i)}}} - 1\right)^{-1}. \tag{18}$$

Those can be used together with (11) and (14) to obtain a range uncertainty for the k-th VA for the given environment.

The SINR estimation described in [6] also performs a correction of deterministic factors such as distance-dependent path-loss. Overall, it leads to sets $\tilde{\mathcal{A}}^{(j)}$ of VAs with lower cardinality than $\mathcal{A}^{(j)}$, consisting of re-estimated VA locations obtained in (15).

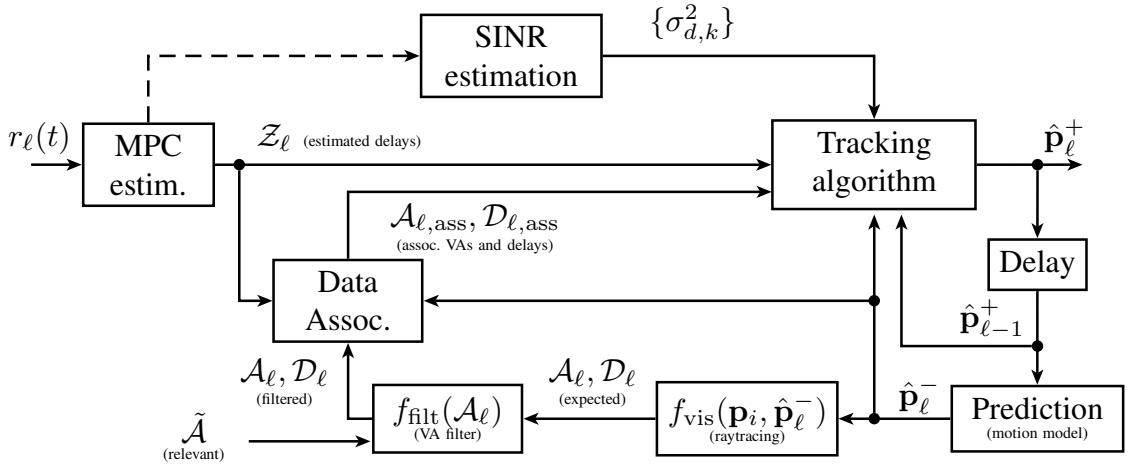

Fig. 2. Block diagram of tracking and data association scheme using MPC range estimates. The estimated MPC delays in the set $\mathcal{Z}_\ell$ are fed to the data association, in which they are associated to the set of expected (and possibly filtered) VAs $\mathcal{A}_\ell$ and the corresponding delays $\mathcal{D}_\ell$. These sets are computed by geometric ray-tracing at the predicted position $\hat{\mathbf{p}}^-_\ell$, based on the knowledge of the room geometry. Optionally, estimated range uncertainties can be used to weight the measurements in the tracking algorithm.

2) Online Estimation using estimated Positions: The estimation technique discussed above can also be performed *during* the tracking phase. The sets of known training points in (13) need to be replaced by the estimated previous positions of the tracking algorithm. Hence, the SINR of the associated MPCs at every position can be updated using window estimates for the moments of the energy samples used in (18). Also, the re-estimation of the VA locations as in (15) is not possible without known agent positions. However, the inclusion of the VA positions in the state vector for an online tracking is out of scope of this paper. The parallel TD [2] discusses these issues amongst others.

3) Performance Prediction based on Channel Information: As discussed in [10], the estimated MPC SINRs (18) can be used together with the known geometry and (10) to obtain an estimate for the so-called position error bound (PEB) [13]

$$\mathcal{P}(\mathbf{p}_\ell) = \sqrt{\mathrm{tr}\left\{\mathbf{J}^{-1}_{\mathbf{p}_\ell}\right\}}. \tag{19}$$

III. Measurement Scenario

Measurements were obtained along a trajectory of 220 points, spaced by 5 cm, see Fig. 1. Around each point, 25 measurements were performed within a 5 x 5 cm grid, yielding in fact 25 parallel trajectories for the performance analysis.

The channel between the agent on the trajectory and two anchors (see Fig. 1) has been measured with an M-sequence based UWB channel sounder developed by *Ilmsens*, as also described in [14]. On anchor and agent sides, dipole-like antennas made of Euro-cent coins have been used. They have an approximately uniform radiation pattern in azimuth plane and zeroes in the directions of floor and ceiling. Out of the measured frequency range of $3.1 - 10.6$ GHz, a subband with center frequency f_c and bandwidth $B = 1/T_\mathrm{p}$ has been selected using filtering with a raised-cosine pulse $s(t)e^{j2\pi f_\mathrm{c} t}$ with pulse duration T_p, followed by a downconversion.

IV. Results

For the tracking along the 25 trajectories, a frequency range corresponding to $f_\mathrm{c} = 7$ GHz and $T_\mathrm{p} = 0.5$ ns has been chosen, which results in a bandwidth of 2 GHz. The process noise variance in the motion model (6) is obtained as in [4] based on selecting a maximum velocity in e.g. the x-direction $v_{x,\max}$, which defines the 3σ point of the noise in velocity domain. The corresponding process noise variance in the acceleration domain is then $\sigma_a^2 = \left(v_{x,\max}/(3\Delta T)\right)^2$ with $v_{x,\max} = 1$ m/s and $\Delta T = 1$ s in this paper. The DA cutoff distance has been chosen as $d_\mathrm{c} = 0.12$ m. VAs up to order two have been used, and SINR estimation was done using $N_\mathrm{seg} = 3$ sets of 20 points (Fig. 1). The prior for the VA positions in (15) has been chosen as a uniform distribution within a circle of diameter 10 cm around the calculated VA position. The performance of the EKF is compared for the cases with estimated SINRs (8), and where no such information is available (9). To allow for a fair comparison in the latter case, the overall ranging uncertainty is selected as the mean of the estimated uncertainties, which is $\sigma_\mathrm{d} = 0.042$ m.

A. Channel Estimation and Performance Prediction

Fig. 3 shows a plot of several received signals between the agent and Anchor 2, which are a subset of the SINR estimation points indicated in Fig. 1. Grey lines mark the amplitude tracks of several deterministic, VA-modeled MPCs. The analysis of the SINR gives insights on important propagation mechanisms in the environment. The LOS component provides a very stable amplitude and thus a large SINR, yielding a very low ranging variance. Other important reflectors that carry significant position-related information are the blackboard on the upper side of the room and the windows (marked in grey in Fig. 1). Multiple reflections between the windows on the right and left side of the room also show a large SINR. Interestingly, this SINR can be larger

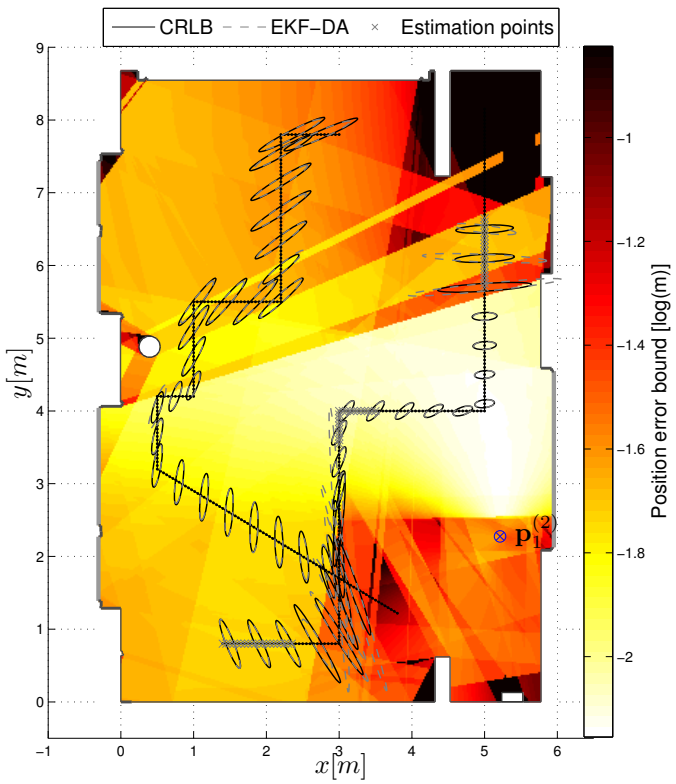

Fig. 4. PEB using estimated SINRs and (10) (neglecting path overlap) with $T_\mathrm{p} = 0.5\,\mathrm{ns}$ and $f_\mathrm{c} = 7\,\mathrm{GHz}$, only Anchor 2 is used for estimation and tracking. The grey crosses are the 60 estimation points for the SINR. The black ellipse denotes the CRLB at some points of trajectory 2. The grey ellipses denote the estimation error covariance matrix of the EKF-DA using estimated measurements noise model (8). All ellipses are enlarged by a factor of 20 for better perceptibility.

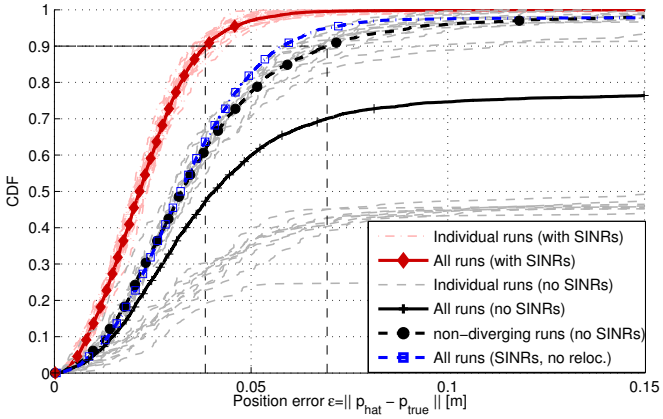

Fig. 5. Performance CDFs for $T_\mathrm{p} = 0.5\,\mathrm{ns}$ and $f_\mathrm{c} = 7\,\mathrm{GHz}$. Thin lines show the individual 25 runs over the trajectories in Fig. 1. Red and gray indicate the EKFs with and without estimated SINRs. Bold lines denote the total performance for all runs, the dashed black line indicates the performance without SINRs on all non-diverging runs (15 out of 25).

than the one corresponding to the right window alone. A look on the corresponding MPC reveals that the first-order reflection is in a region of the signal with a large amount of DM, causing a moderate SINR, which can be evaluated using the estimation technique. For higher-order interactions involving this MPC and another, well reflecting surface such as the left window, the excess delay is much larger. Hence, the influence of DM may be decreased for these components, which leads to a larger SINR.

Fig. 3 also shows the mean and standard deviation of the energy capture (EC) of all the VA-modeled MPCs w.r.t the received signal, estimated at all 60 training positions [15]. It can be seen (also for other measurements) that energetic considerations may not directly translate to information measures, such as the CRLB. For example, the MPC corresponding to the right window contains significant energy, but a relatively low SINR, i.e. position-related information.

The estimated SINRs and the geometry can be used with (19) to predict the localization performance. The calculated logarithmic PEB using the estimated SINRs for only Anchor 2 (c.f. Fig. 3) is presented in Fig. 4. It can be observed that the expected localization performance is better than 10 cm throughout most of the room, despite the fact that only one anchor is used. Tracking results in terms of standard deviation ellipses (enlarged by a factor of 20) corresponding to the EKF state estimation covariance matrix confirm that the CRLB can actually be achieved with the presented algorithms. These observations could be confirmed in other scenarios where we have obtained measurements [10], [16].

B. Tracking Results

An exemplary tracking result is illustrated in Fig. 1. In this case, the EKF can track the agent with and without estimated MPC SINRs, also in the NLOS region with respect to Anchor 1 (caused by the concrete pillar on the left side of the room). At every 12-th position, the 20-fold estimation error standard deviation ellipse of the EKF is illustrated. The comparison with the estimated CRLB, given as the inverse of (10), shows a close match to the tracking performance when using the SINRs, which confirms the efficient use of the MPCs. It should be noted that the CRLB shown does not include the motion model, i.e. it is not the posterior CRLB. However, for the chosen process noise variance, which is deliberately larger than the measurement uncertainties, the motion prior does not add significant information, making (10) applicable.

Fig. 5 shows the position error CDFs. It is evident that the channel characterization (red) yields excellent robustness, as all 25 runs have similar performance with 90 % of the errors below 4 cm. Without SINR information (black/gray), the robustness is affected, as 10 of 25 runs diverge, mostly in the NLOS region discussed before. The overall CDF for the 15 non-diverging runs (black bold dashed line, circle markers) shows the *potential* performance of MINT without channel information, where 90 % of the errors are within 7 cm. The influence of the MAP-re-localization of the VA positions (15) is illustrated by the CDF indicated by the blue dash-dotted curve with square markers. All runs are included, SINRs used, but without the re-localized VA positions. SINR awareness provides robustness, while re-localization improves accuracy.

Fig. 6 illustrates the mean number of associated MPCs,

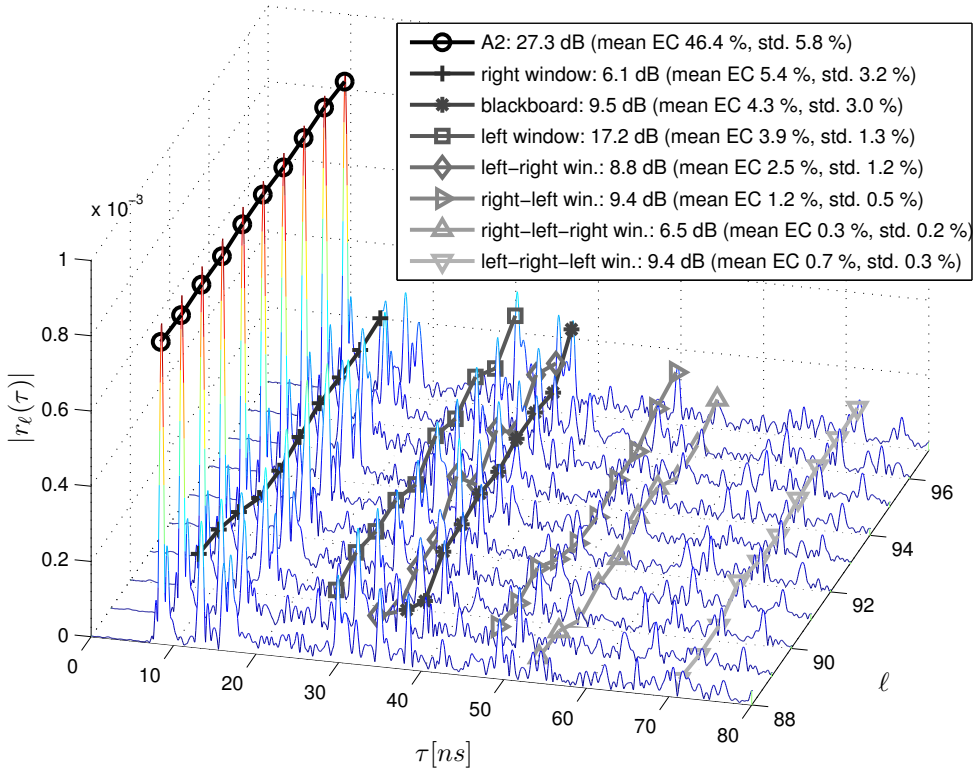

Fig. 3. Estimated SINRs over the estimation points on trajectory 1 indicated in Fig. 4 using Anchor 2 and $T_\mathrm{p} = 0.5\,\mathrm{ns}$ and $f_\mathrm{c} = 7\,\mathrm{GHz}$. Amplitude tracks are shown for a subset of the estimation points. Besides the SINR, also the mean energy capture w.r.t. the whole received signal [10], [15] and its standard deviation over all estimation points are indicated.

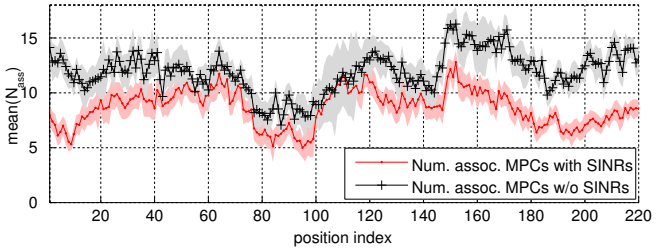

Fig. 6. Mean and standard deviation of the number of associated MPCs used for tracking. The 15 of 25 non-diverging runs are included for the case where no SINRs are available.

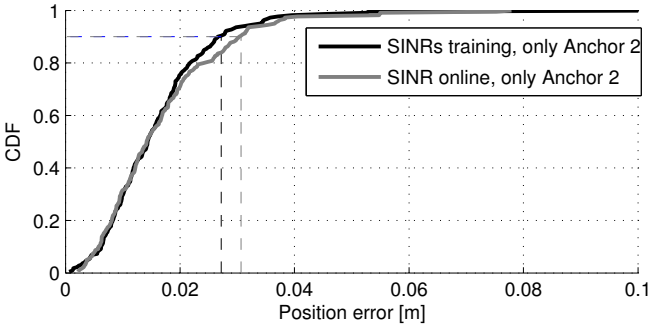

Fig. 7. Performance CDFs for $T_\mathrm{p} = 0.5\,\mathrm{ns}$ and $f_\mathrm{c} = 7\,\mathrm{GHz}$ using only anchor 2. For the black line, the estimated SINRs are used to weight the measurements in the EKF, for the grey one, the SINRs have been estimated online using the estimated positions.

$\mathbb{E}\{|\mathcal{A}_{\ell,\mathrm{ass}}|\}$, over all runs using SINRs and the 15 non-diverging runs without SINRs, together with the standard deviation. The additional channel knowledge helps to substantially prune the set of potential VAs to the relevant ones. This leads to less erroneous associations of estimated MPCs to VAs and also reduces the computational complexity.

C. Online Variance/SINR Estimation

Fig. 7 shows CDFs of the tracking error for single anchor tracking with only Anchor 2, both for SINRs estimated on training data and for online estimated SINRs. Also in addition to the results in Fig. 5, a 5-fold oversampling of the signals has been used to increase the ranging accuracy. A performance of 90 % of the errors within roughly 3 cm can be achieved in both cases, where the online estimation makes no use of a-priori estimated SINRs.

Fig. 8 shows exemplary values for the estimated ranging standard deviations. It can be observed that in general, the offline estimated values are good global indicators for the general weighting of the MPCs, which explains their usefulness. For each MPC, the online estimation results are only shown for those positions, for which an estimation could be done, based on both visibility of the MPCs as well as on the estimation results. Of course the online SINR estimation is only useful as long as the tracking filter is on track.

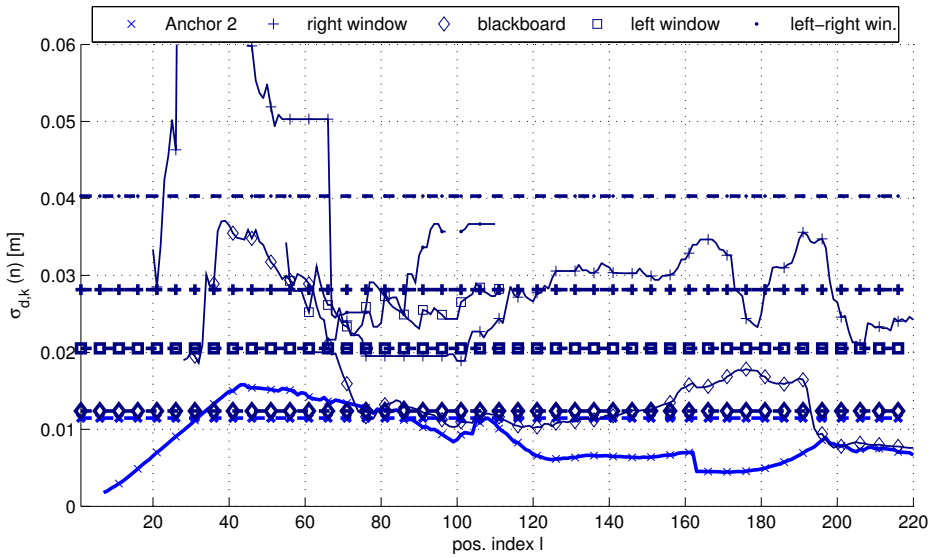

Fig. 8. Standard deviations of the ranging to selected MPCs using $T_\mathrm{p} = 0.5\,\mathrm{ns}$ and $f_\mathrm{c} = 7\,\mathrm{GHz}$ using only anchor 2, i.e. corresponding to the CDF in Fig. 7. For dashed bold lines, the SINRs are estimated using training signals at known positions (see Fig. 1, for the thin solid lines, they have been online using the estimated positions.

V. Conclusions

We have shown that channel knowledge quantifying the position-related information of deterministic MPCs is a key factor for obtaining accurate and robust indoor localization. By estimating the uncertainty of range estimates corresponding to deterministic MPCs and making this information available to a tracking filter, multipath propagation can be used efficiently. Experimental results have confirmed the advantage, demonstrating excellent performance.

References

[1] P. Meissner, E. Leitinger, and K. Witrisal, "UWB for Robust Indoor Tracking: Weighting of Multipath Components for Efficient Estimation," *IEEE Wireless Communications Letters*, vol. 3, no. 5, pp. 501–504, Oct. 2014.

[2] E. Leitinger, P. Meissner, M. Lafer, and K. Witrisal, "Multipath-assisted Indoor Simultaneous Localization and Mapping," in *COST Action IC1004 Scientific Meeting*, Dublin, Ireland, 2015.

[3] D. Dardari, A. Conti, U. Ferner, A. Giorgetti, and M. Z. Win, "Ranging With Ultrawide Bandwidth Signals in Multipath Environments," *Proceedings of the IEEE*, 2009.

[4] P. Meissner, E. Leitinger, M. Froehle, and K. Witrisal, "Accurate and Robust Indoor Localization Systems Using Ultra-wideband Signals," in *European Navigation Conference (ENC)*, Vienna, Austria, 2013. [Online]. Available: http://arxiv.org/abs/1304.7928

[5] K. Witrisal and P. Meissner, "Performance bounds for multipath-assisted indoor navigation and tracking (MINT)," in *International Conference on Communications (ICC)*, Ottawa, Canada, 2012.

[6] P. Meissner and K. Witrisal, "Analysis of Position-Related Information in Measured UWB Indoor Channels," in *6th European Conference on Antennas and Propagation (EuCAP)*, Prague, Czech Repuplic, 2012, convened session.

[7] Y. Shen, S. Mazuelas, and M. Win, "Network Navigation: Theory and Interpretation," *IEEE Journal on Selected Areas in Communications*, 2012.

[8] A. Conti, D. Dardari, M. Guerra, L. Mucchi, and M. Win, "Experimental Characterization of Diversity Navigation," *IEEE Systems Journal*, 2014.

[9] N. Decarli, F. Guidi, and D. Dardari, "A Novel Joint RFID and Radar Sensor Network for Passive Localization: Design and Performance Bounds," *IEEE Journal of Selected Topics in Signal Processing*, 2014.

[10] P. Meissner, "Multipath-Assisted Indoor Positioning," Ph.D. dissertation, Graz University of Technology, 2014.

[11] J. Kunisch and J. Pamp, "An ultra-wideband space-variant multipath indoor radio channel model," in *IEEE Conference on Ultra Wideband Systems and Technologies*, 2003.

[12] D. Schuhmacher, B.-T. Vo, and B.-N. Vo, "A Consistent Metric for Performance Evaluation of Multi-Object Filters," *IEEE Transactions on Signal Processing*, 2008.

[13] Y. Shen and M. Z. Win, "Fundamental Limits of Wideband Localization - Part I: A General Framework," *IEEE Transactions on Information Theory*, 2010.

[14] P. Meissner, E. Leitinger, M. Lafer, and K. Witrisal, "Real-Time Demonstration System for Multipath-Assisted Indoor Navigation and Tracking (MINT)," in *IEEE ICC Workshop on Advances in Network Localization and Navigation (ANLN)*, Sydney, Australia, 2014.

[15] M. Win and R. Scholtz, "Characterization of ultra-wide bandwidth wireless indoor channels: A communication-theoretic view," *IEEE Journal on Selected Areas in Communications*, vol. 20, no. 9, pp. 1613 – 1627, Dec. 2002.

[16] P. Meissner, E. Leitinger, M. Lafer, and K. Witrisal, "MeasureMINT UWB database," www.spsc.tugraz.at/tools/UWBmeasurements, 2013, Publicly available database of UWB indoor channel measurements. [Online]. Available: www.spsc.tugraz.at/tools/UWBmeasurements